Journal of Science and Technology in Civil Engineering, HUCE, 2025, 19 (1): 72–92

STUDY ON SPATIAL ARRANGEMENT FOR COASTAL PROTECTION SOLUTIONS IN BEN TRE PROVINCE USING NUMERICAL MODEL

Vu Minh Tuan[a,*], Ngo Quang Bao Hoang[b]

[a]*Faculty of Hydraulic engineering, Hanoi University of Civil Engineering, 55 Giai Phong road, Hai Ba Trung district, Hanoi, Vietnam*
[b]*Coastal & River engineering research center, Portcoast Consultant Corporation, 92 Nam Ky Khoi Nghia, district 1, Ho Chi Minh City, Vietnam*

Article history:
Received 12/02/2025, Revised 08/3/2025, Accepted 17/3/2025

Abstract

The coastline of Ben Tre Province, situated between the major estuaries of the Mekong River system, stretches approximately 65 km and has been experiencing severe erosion in recent years. Some single shore protection structures were built to protect severely eroded areas. While these structures show certain protective effectiveness, erosion continues to occur along other sections. This study focuses on the characteristics of the hydrodynamic regime and sediment transport along the entire coast of Ben Tre province as well as the impact of spatial arrangement of protection solutions on local hydrodynamics and sedimentation. The MIKE 21 numerical model is employed to simulate and evaluate coastal morphological changes under the proposed spatial arrangement of detached breakwaters combined with T-shaped groynes under different monsoon scenarios and the historical Linda storm. The simulation results indicate that the deployment of these structures not only significantly reduces wave energy and current speed but also promotes sediment deposition in the sheltered areas behind the structures.

Keywords: Ben Tre; erosion; accretion; numerical model; spatial arrangement; coastal protection structures.

https://doi.org/10.31814/stce.huce2025-19(1)-07

1. Introduction

The coastline serves as the boundary between land and ocean, hosting a diverse ecosystem and providing significant value for socio-economic development. However, in recent years, the combined effects of natural and human factors, along with sea level rise due to climate change, have caused erosion to dominate over accretion, resulting in significant changes to the coastal morphology [1]. Ben Tre Province, located in southern Vietnam and in the Mekong Delta region (Fig. 1), is no exception to this trend. Currently, nearly 20 km of coastline in Thanh Phu, Ba Tri, and Binh Dai districts are experiencing erosion, with increasingly complex patterns [2]. Statistics show eight erosion hotspots totaling approximately 19.4 km, including three severely eroded sections exceeding 5 km. Additionally, alternating erosion and accretion zones shift with the Northeast and Southwest monsoons along Ben Tre's coast. To halt erosion, several structural measures were implemented along certain coastal areas in Cho Lach, Ba Tri, and Thanh Phu districts. While these coastal protection structures have initially proven effective, their construction and arrangement remain localized, reactive, and fragmented, primarily relying on experience without a comprehensive strategy for the province's entire coastline. Furthermore, these measures are predominantly reactive. In the long term, proactive solutions that

*Corresponding author. *E-mail address:* tuanvm@huce.edu.vn (Tuan, V. M.)

adapt to climate change are necessary. Therefore, a comprehensive coastal regulation and stabilization strategy for the entire province is essential to maximize the effectiveness of these structures and ensure sustainable coastal protection.

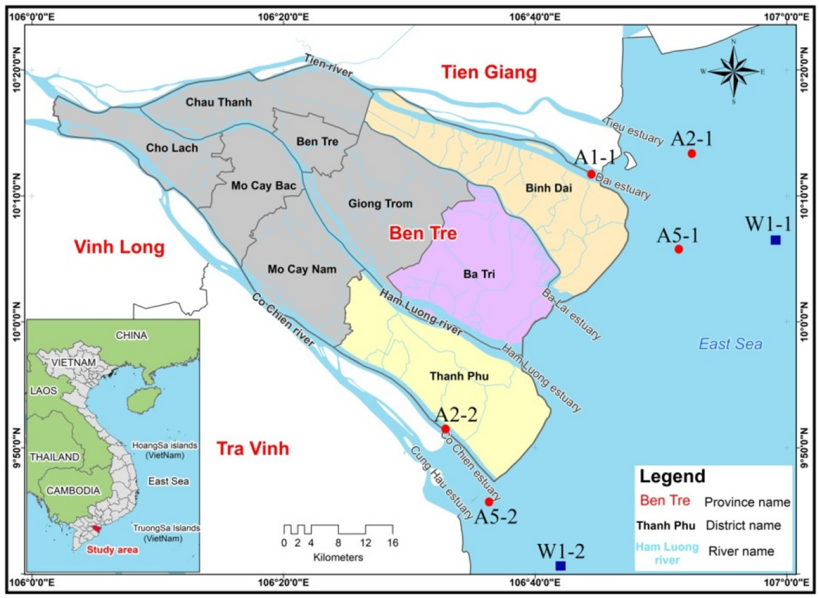

Figure 1. Study area and location of measuring stations

2. Data and Methods

2.1. Input data

The bathymetry of the computational domain for the Mekong Delta river system is obtained from data provided by the Mekong River Commission. The coastal bathymetry is compiled from field survey results. For offshore areas, the bathymetric data is sourced from the General Bathymetric Chart of the Oceans (GEBCO) [3]. Flow discharge data for the Tien River and Hau River in 2020 were collected at the My Thuan and Can Tho stations, respectively. Offshore wave and wind data were collected from the European Center for the Medium-Term Weather Forecasts (ECMWF) [4] model at a depth of around 38 meters. The wave rose and wind rose diagrams for 21 years (2002–2022) offshore of Ben Tre province are presented in Fig. 2 and Fig. 3.

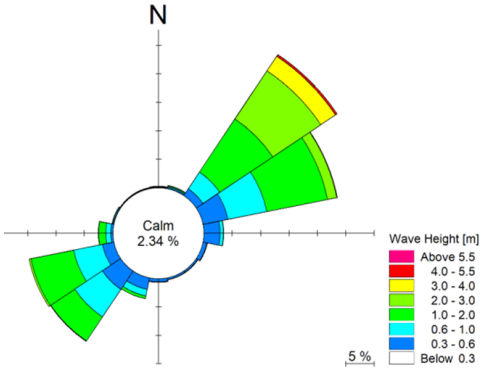

Figure 2. Wave rose in 2002 – 2022 [4]

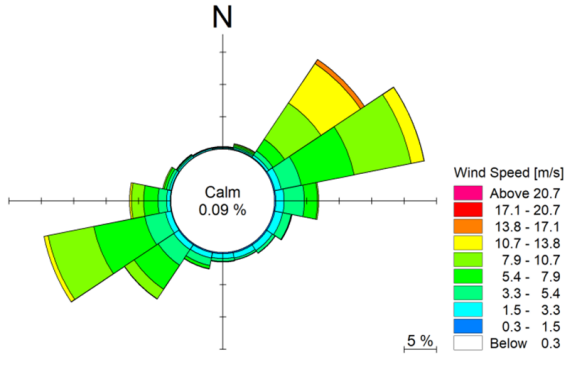

Figure 3. Wind rose in 2002 – 2022 [4]

Storms are rare in the study area, with the most significant recorded event being Linda storm in 1997. The maximum wind speed caused by Linda storm reached approximately 30 m/s [5].

2.2. *Descriptions of Numerical Models*

To evaluate the impact of spatial arrangements of coastal protection solutions on hydrodynamics and sediment transport in Ben Tre province, the MIKE 21 modeling suite was employed, including MIKE 21 HD [6], MIKE 21 SW [7], and MIKE 21 MT [8]. Specifically, the MIKE 21 SW model was applied to simulate wave propagation from deep offshore water to shallow nearshore areas. Meanwhile, the MIKE 21 HD model was used to simulate wave-induced currents and water level fluctuations, and the MIKE 21 MT model was utilized to simulate cohesive sediment transport.

The study area covers the coastal region of Ben Tre province, extending from the Ba Ria - Vung Tau coastal zone to the Soc Trang coastal zone (Fig. 4). It stretches upstream along the rivers to the My Thuan station (Tien River) and Can Tho station (Hau River). The offshore boundary is located approximately 140 km from the shoreline, encompassing areas with water depths primarily under 40 meters. A hybrid computational grid was employed, consisting of a structured quadrilateral grid for riverine and estuarine areas, and an unstructured triangular grid for coastal and offshore regions. The entire grid comprises 52,512 nodes and 82,174 elements. The smallest element area is about 50 m^2 inside the river and along the beaches, while the largest element area is about 52 km^2 in the offshore area (Fig. 4).

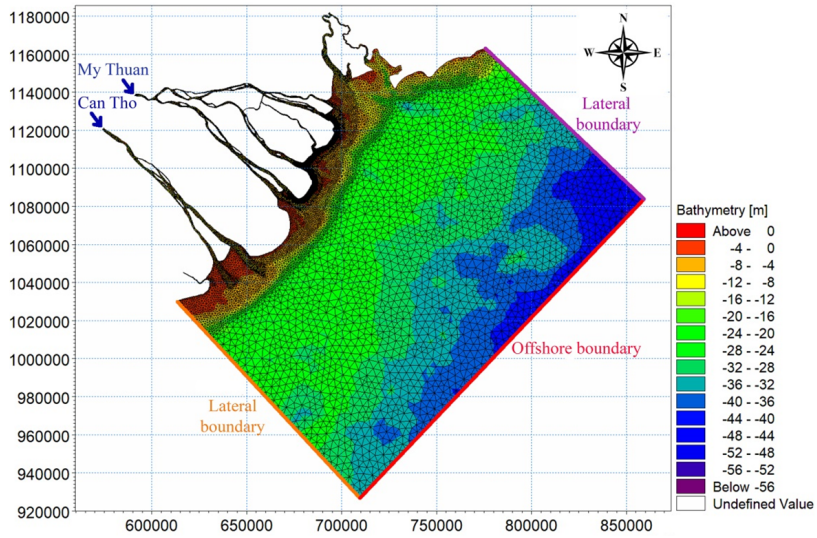

Figure 4. Computational mesh domain

2.3. *Model parameters*

The agreement between simulated and observed data is evaluated using key statistical parameters, including Root Mean Square Error (*RMSE*), R-squared (R^2), the Index of Agreement (d), and the Nash–Sutcliffe Model Efficiency Coefficient (*NSE*) [9, 10]. In the MIKE 21 HD numerical model, bed resistance is defined using the Manning's number, which can vary depending on water depth and bed surface characteristics [11, 12]. The final Manning's number in the computational domain is determined to achieve the best match between calculated flow/water levels and observed data. Similarly, the MIKE 21 SW model is calibrated by adjusting the Nikuradse roughness length (k_n), which is a function of the mean particle diameter (D_{50}) of the sediment in the study area [12]. For

the MIKE 21 MT model, two parameters of critical bed shear stress for erosion (τ_{ce}) and critical bed shear stress for deposition (τ_{cd}) are selected to adjust the calculated and observed suspended sediment concentrations [13, 14].

2.4. Simulation scenarios

The first step in developing the modeling scenarios is to arrange the spatial layout of coastal protection solutions for the entire eroding coastline of Ben Tre province. Based on the results of field analysis and the synthesis of experiences from previous coastal protection projects [2, 15, 16] in the Mekong Delta, the authors proposed the use of T-shaped groyne and detached breakwater systems for the study area. The dimensions of the groynes and detached breakwaters were determined according to formulas proposed by Dally et al. [17]. Specifically, the T-shaped groynes have a body length of 300 m and wing lengths of 200 m, while the detached breakwaters are 200 m long and placed 300 m from the shoreline. The gap between the two modules was selected based on the recommendations of Seiji et al. [18] to prevent the creation of erosion channels, with a distance of 160 m. The crest width of both the T-shaped groynes and detached breakwaters is set to 8 m, according to the recommendation of Tanaka [19]. The results are shown in Fig. 5.

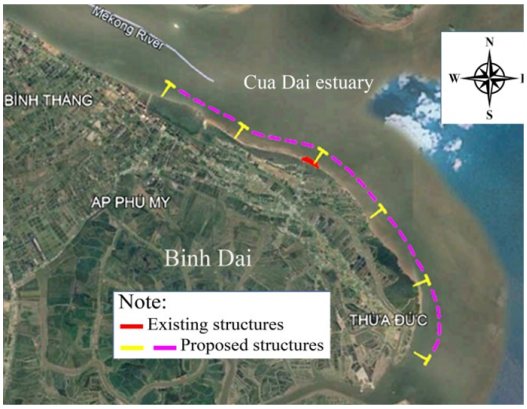

(a) Segment A (Thua Duc Commune, Binh Dai District)

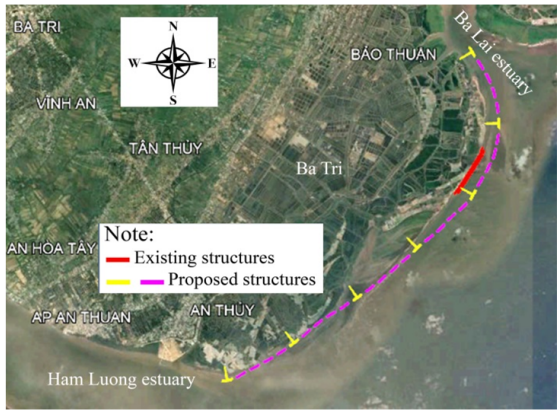

(b) Segment B (Bao Thuan and An Thuy communes, Ba Tri District)

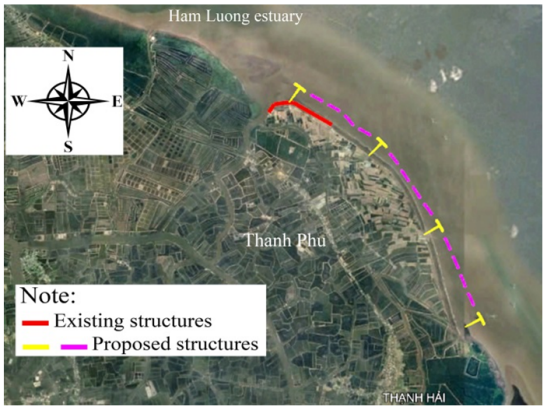

(c) Segment C (Thanh Hai commune, Thanh Phu District)

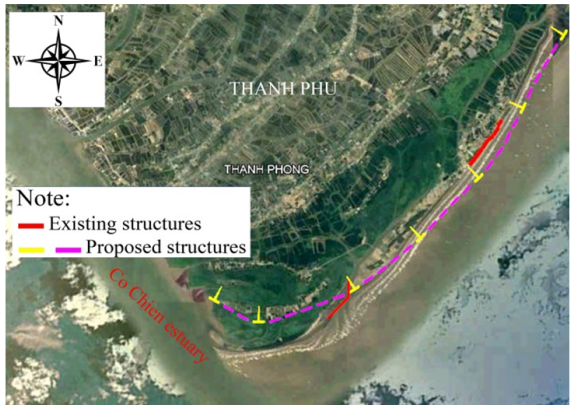

(d) Segment D (Thanh Phong Commune, Thanh Phu District)

Figure 5. Spatial arrangement of regulation solutions along the Ben Tre coastline

The impact of the spatial layout of coastal protection measures in the study area will be clarified and quantified through simulations of different wave conditions, including the Northeast monsoon (NE), Southwest monsoon (SW), and the historical Linda storm (Linda). In the NE and SW scenarios, the selection of representative months for the Northeast and Southwest monsoon seasons is based on the analysis of offshore wave and wind data collected over many years. Tide and river discharge data were chosen based on monthly observation data. For Linda scenario, the historical Linda storm (1997) is selected as a representative storm. Details of the study scenarios are shown in Table 1.

Table 1. Details of the research scenarios

Notation	Case	Note
NE0	NE monsoon wind without protection system	Current Situation
NE1	NE monsoon wind with protection system	With groynes and breakwaters
SW0	SW monsoon wind without protection system	Current Situation
SW1	SW monsoon wind with protection system	With groynes and breakwaters
Linda0	Linda storm without protection system	Current Situation
Linda1	Linda storm with protection system	With groynes and breakwaters

3. Model verification

To evaluate the performance of the hydrodynamic and sediment transport models with different types of data, the simulation results were compared with observed data at several locations within the computational domain (Fig. 1). Model calibration was conducted during the period from December 2019 to January 2020 at stations of W1-1, A1-1, A2-1, and A5-1. Meanwhile, model validation was carried out at stations of W1-2, A2-2, and A5-2 during April 2020.

3.1. Model calibration

The results of the hydrodynamic model calibration showed a high degree of agreement between observed and simulated data in terms of both phase and amplitude (Table 2, Fig. 6, and Fig. 7). In this study, water level and current were considered to evaluate the performance of the hydrodynamic model due to the complex geographical and geometrical features of the Mekong estuaries. To calibrate the sediment transport model, simulation results were compared with field data from three stations of A1-1, A2-1, and A5-1 during December 2019 and January 2020. Fig. 8 shows that most suspended sediment concentration (SSC) simulations closely match the observations, although some discrepancies in amplitude and phase still exist at these stations.

Table 2. Statistical errors in the calibration and validation of models

Parameter	*RMSE*	*d*	R^2	*NSE*
Water level at station W1-1	0.32	0.96	0.88	0.86
Current speed at station W1-1	0.05	0.90	0.82	0.51
Current direction at station W1-1	38.21	0.90	0.80	0.44
Wave height at station W1-1	0.32	0.86	0.61	0.43
Wave period at station W1-1	0.87	0.63	0.38	−0.56
Wave direction at station W1-1	5.43	0.54	0.11	−0.39
SSC at station A1-1	0.08	0.40	0.01	−1.41
SSC at station A2-1	0.05	0.78	0.46	0.05
SSC at station A5-1	0.09	0.79	0.59	−0.27

Parameter	*RMSE*	*d*	R^2	*NSE*
Water level at station W1-2	0.25	0.97	0.90	0.90
Current speed at station W1-2	0.08	0.89	0.71	0.41
Current direction at station W1-2	77.45	0.69	0.14	−0.42
Wave height at station W1-2	0.31	0.92	0.84	0.70
Wave period at station W1-2	0.68	0.82	0.56	0.05
Wave direction at station W1-2	20.97	0.57	0.30	−0.80
SSC at station A2-2	0.07	0.58	0.15	−1.51
SSC at station A5-2	0.08	0.45	0.04	−2.77

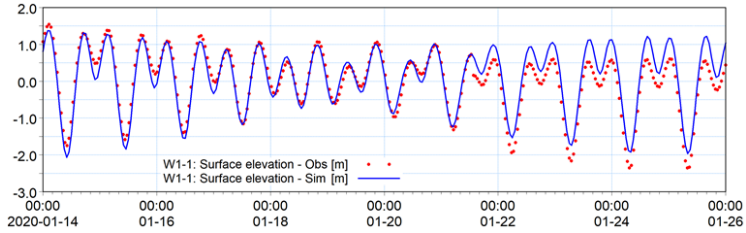

(a)

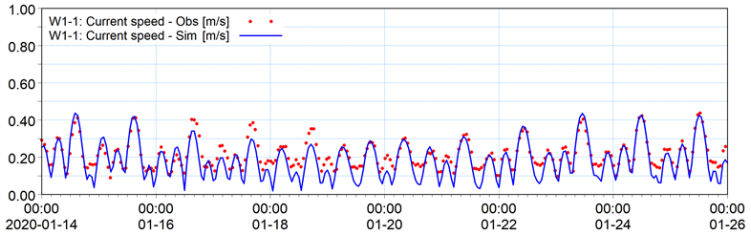

(b)

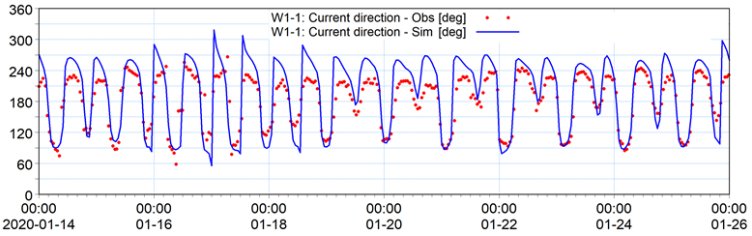

(c)

Figure 6. Comparison of simulated and measured water level fluctuations (a); current speed (b); and direction (c) at station W1-1

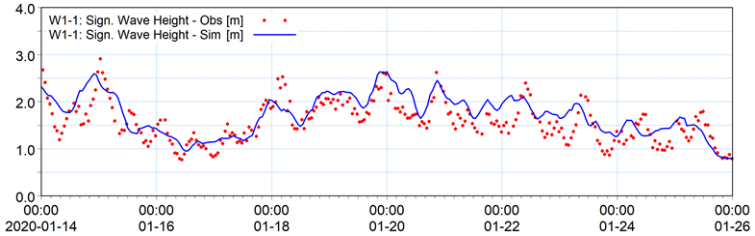

(a)

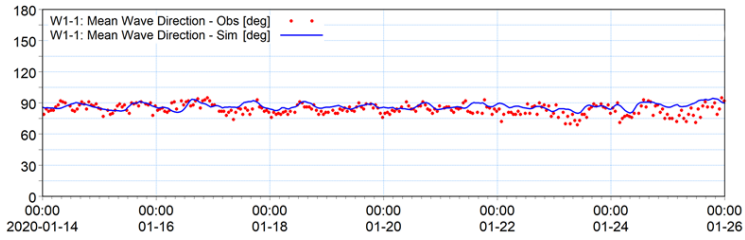

(b)

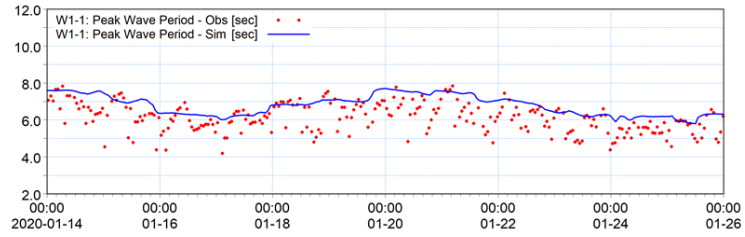

(c)

Figure 7. Comparison of simulated and measured wave height (a); period (b); and direction (c) at station W1-1

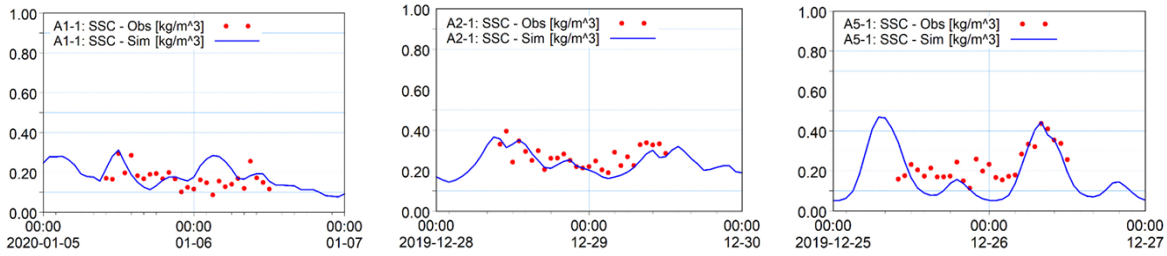

(a) (b) (c)

Figure 8. Comparison of simulated and measured SSC at stations of A1-1 (a); A2-1 (b); and A5-1 (c)

3.2. Model validation

The validation results, based on observed data from the Mekong River estuary stations, are presented in Figs. 9, 10, and 11. While some discrepancies remain between the observed data and the model results, the overall accuracy of the model is acceptable, and the simulations reasonably capture the general trends in water level, current, wave dynamics, and sediment transport. Table 2 also provides an evaluation of the model's performance in simulating current, wave conditions, and SSC. The comparison shows that the model results align well with the observational data, indicating that the models provide a good representation of the hydrodynamic and sediment transport processes in the study area.

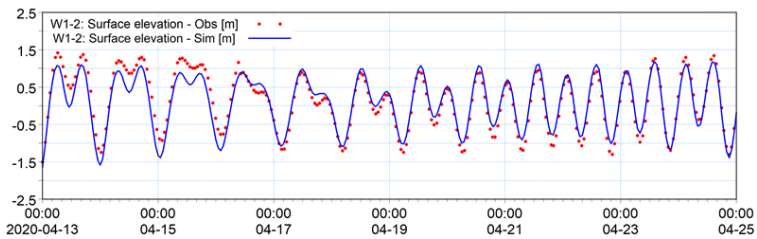

(a)

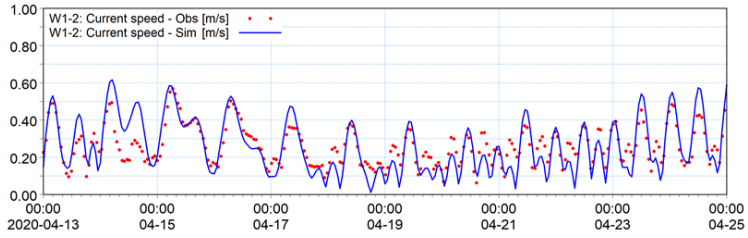

(b)

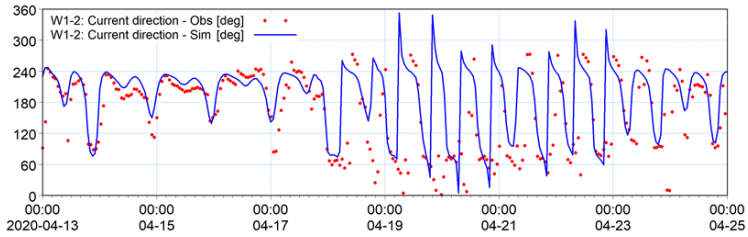

(c)

Figure 9. Comparison of simulated and measured water level fluctuations (a); current speed (b); and direction (c) at station W1-2

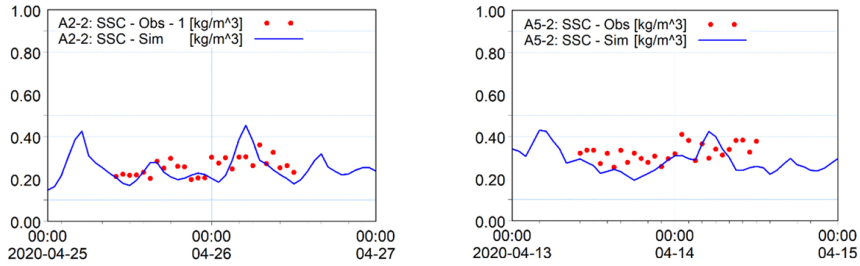

(a) (b)

Figure 10. Comparison of simulated and measured SSC at stations of A2-2 (a) and A5-2 (b)

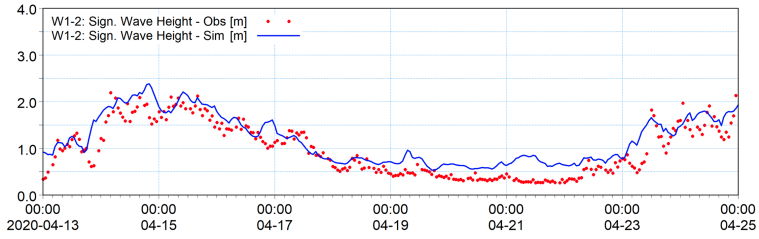

(a)

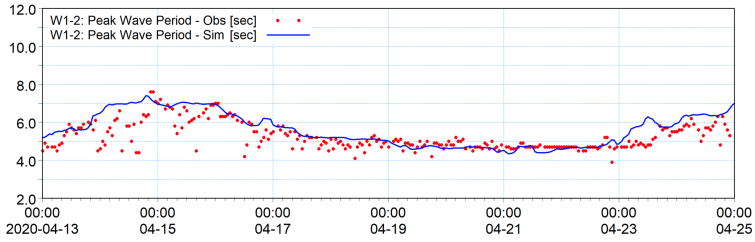

(b)

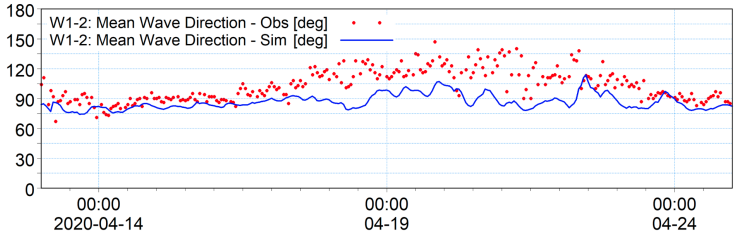

(c)

Figure 11. Comparison of simulated and measured wave height (a); period (b); and direction (c) at station W1-2

4. Results and Discussion

To clarify the impact of the spatial arrangement of protection system, simulation data was extracted at some key points surrounding the structures (Fig. 12).

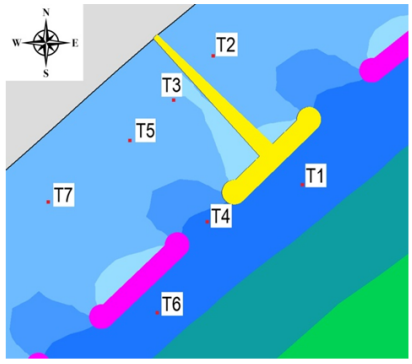

Figure 12. Extraction points around coastal protection structures

4.1. Impact of Protection Solutions on Wave Fields

The simulation results of the wave in the coastal area of Segment A without and with protection system, are presented in Fig. 13. In this segment, the presence of the protection structures significantly reduces wave height and current speed affecting the coastal area. During the NE monsoon season, the wave height behind the structures is reduced from 50% to 75% (Figs. 13(a) and (b)), compared to the current situation. Meanwhile, most of this area is naturally protected from SW waves due to its geographic location and coastal morphology. However, the presence of the structure system also reduced the wave height from 40% to 80% in SW winds (Figs. 13(c) and (d)). In the Linda storm, wave heights of up to 1.8 m propagate close to the shoreline in the current situation. The presence of the structures significantly mitigates wave heights behind the structures reducing to below 0.8 m, corresponding to about 60% (Figs. 13(e) and (f)). The largest wave reduction is observed behind the T-shaped groyne at T2 point, where wave heights during the NE monsoon decrease from 1.3 m to 0.3 m (about 77%), and during storm condition, from 1.6 m to 0.4 m (about 75%).

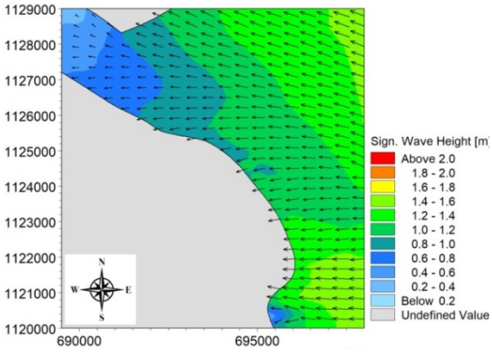

(a) NE0

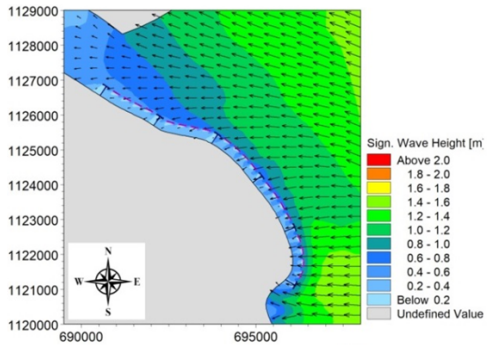

(b) NE1

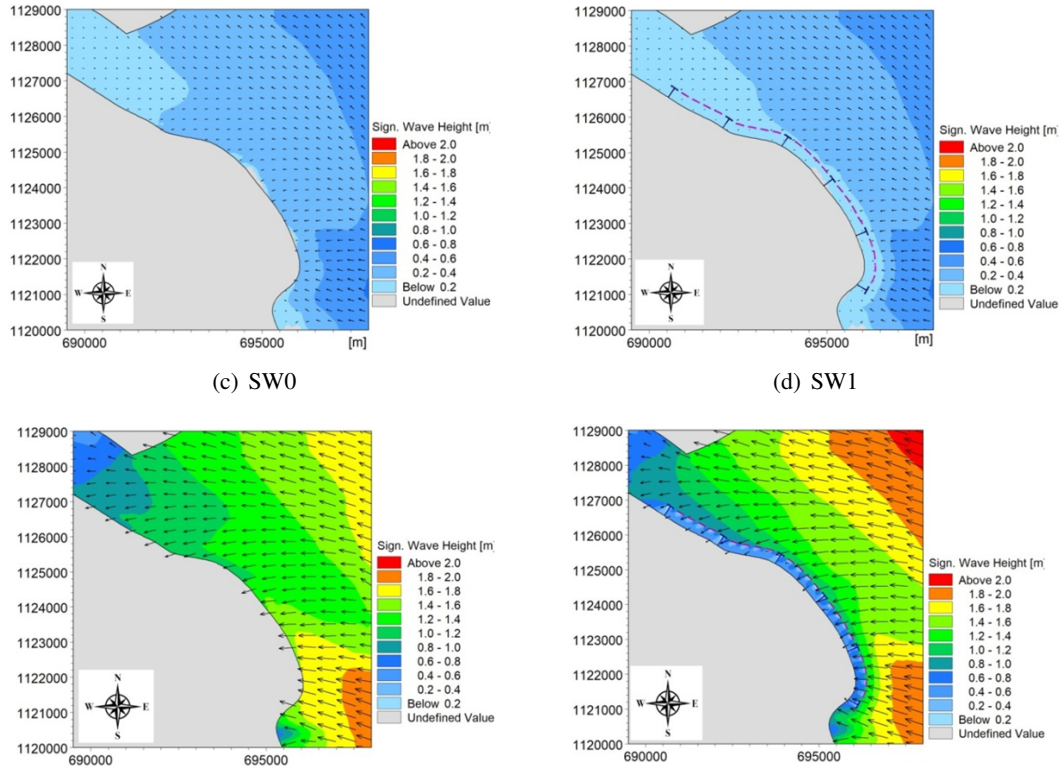

(c) SW0 (d) SW1

(e) Linda0 (f) Linda1

Figure 13. Wave fields in Segment A without and with protection system

Similar to the coastline of Segment A, the presence of the structure system significantly decreases wave heights affecting both Segment B and C. Specifically, in Segment B, wave heights along the shoreline decrease from 67% to 75% in the NE monsoon (Figs. A.1(a) and (b)), from 0.6 m to 0.1 m (about 75%) in the SW monsoon (Figs. A.1(c) and (d)), and from 19% to 73% in storm condition (Figs. A.1(e) and (f)). For Segment C, wave heights behind the breakwater decrease by up to 73% during the NE monsoon (Figs. A.4(a) and (b)), up to 67% in the SW monsoon (Figs. A.4(c) and (d)), and from 57% to 71% in the Linda storm (Figs. A.4(e) and (f)).

The coastal section of Segment D affected by the waves has a much higher height than other areas. Without protection system, this area is significantly impacted by waves, with wave heights at lee-side points (T2, T3, T5, and T7) reaching up to 1.8 m in the NE monsoon (Fig. A.7(a)) and more than 2 m in current conditions (Fig. A.7(e)). The main cause of this phenomenon may be due to its geomorphology. This segment situates near the Co Chien estuary and extends furthest into the sea compared to other study areas. However, the arrangement of protective structures induces a reduction of wave heights about 82% in the NE monsoon (Fig. A.7(b)), from 67% to 86% in the SW monsoon (Fig. A.7(d)) and from 55% to 80% in the Linda storm scenario (Fig. A.7(f)).

4.2. Impact of Protection Solutions on Current Fields

Regarding the current field, the presence of the structures causes the flow to be pushed further offshore in all areas in all simulation scenarios. The current speed in the leeside of the structures decreases from 30% to 80% in Segment A (Fig. 14), up to 86% in Segment B (Fig. A.2), about 80% in Segment C (Fig. A.5), and up to 75% in Segment D (Fig. A.8). Despite the decrease in velocity,

the area behind the protective structures still maintains low currents, with velocities varying below 0.2 m/s. These low currents play a crucial role in facilitating water and sediment exchange between the inside and outside of the structures, helping to prevent stagnation of water. For points outside the structure and between the breakwaters (T1, T4, and T6), current speed values remain almost unchanged compared to the current situation in Segment A, B, and C. However, current velocities at these points decrease by 33% in Segment D.

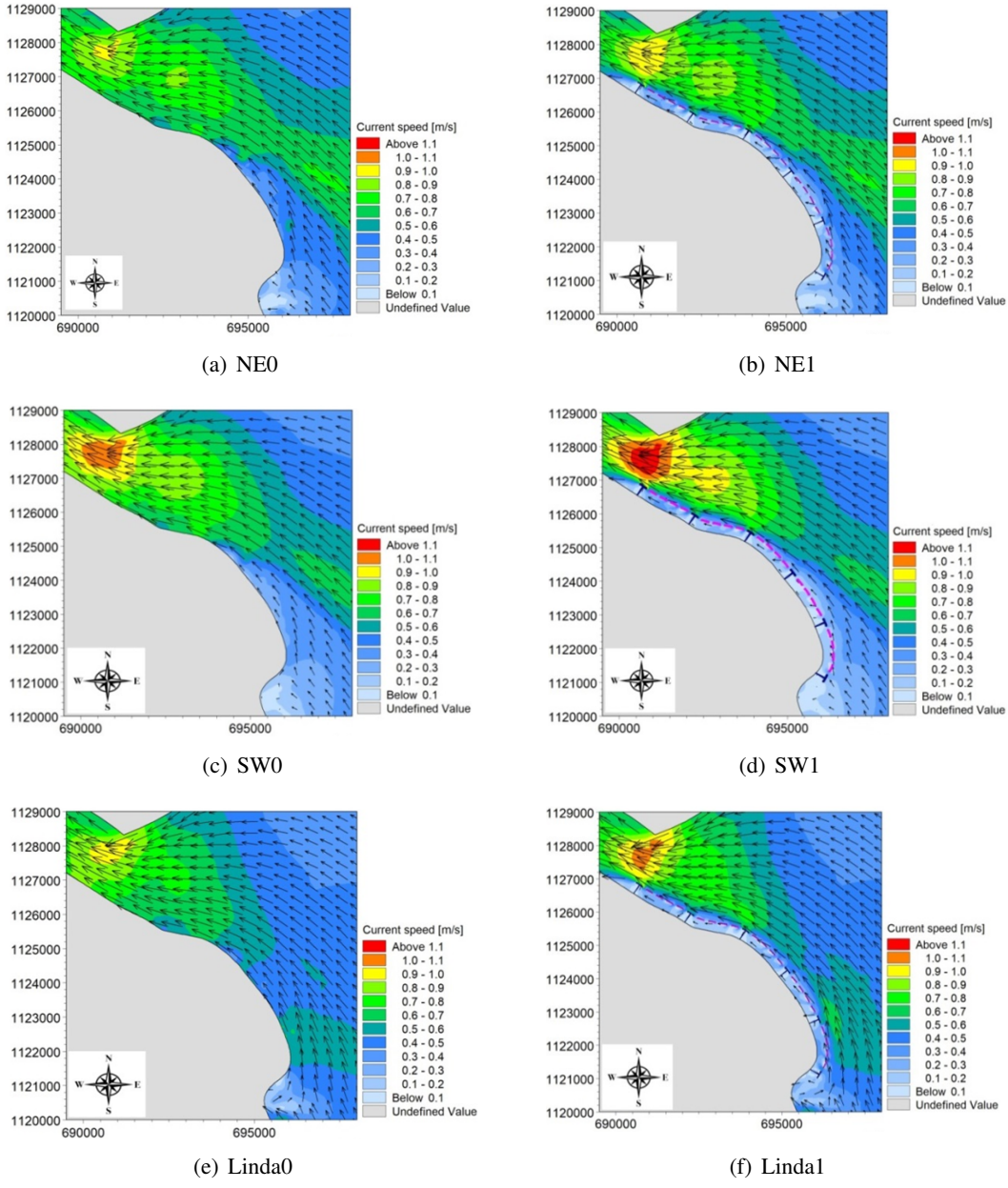

(a) NE0

(b) NE1

(c) SW0

(d) SW1

(e) Linda0

(f) Linda1

Figure 14. Current field in Segment A during high tide without and with protection system

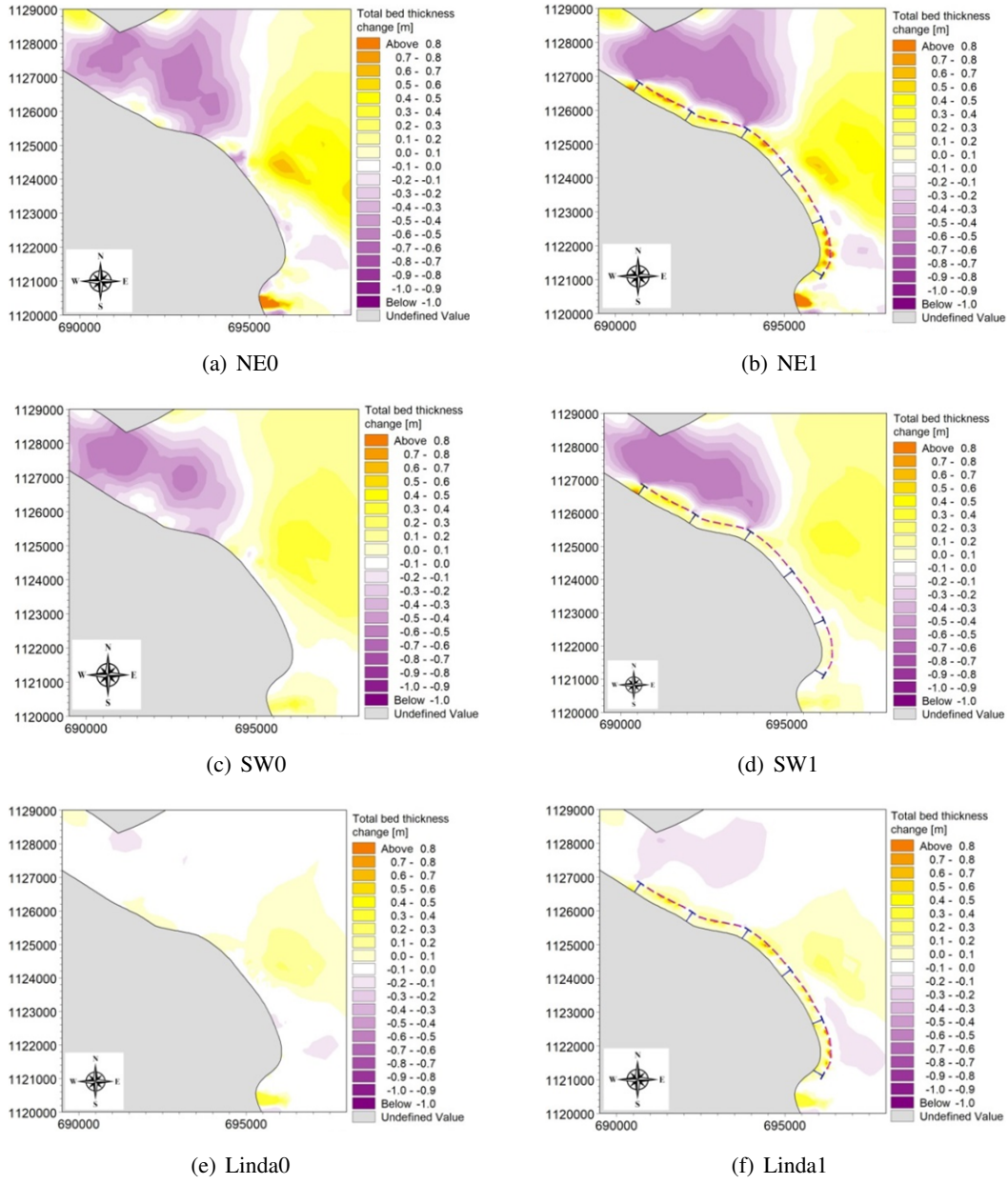

(a) NE0 (b) NE1

(c) SW0 (d) SW1

(e) Linda0 (f) Linda1

Figure 15. Bed level changes around Segment A without and with protection system

4.3. Impact of Protection Solutions on Sedimentation Fields

The simulation results for the seabed erosion and deposition patterns in the coastal area of Segment A are depicted in Fig. 15. During both monsoon periods, erosion occurs along the coastline of Thua Duc commune (the northern areas of this segment), with the seabed erosion thickness varying from 1 to 5 cm. The presence of the protective structures induces sediment deposition behind them. In the NE monsoon, deposition thickness ranges from 1 to 8 cm, with some areas immediately behind the detached breakwater showing an acretion thickness of up to 12 cm (Fig. 15(a)). In the SW monsoon, deposition behind the breakwaters ranges from 1 to 5 cm. At the T-shaped groyne near the Tien river mouth, deposition thickness increases to 8 cm behind the structure (Fig. 15(b)). However,

the presence of the structures also triggers seabed erosion in the estuary area. The seabed thickness in front of these structures decreases by about 5 cm. This phenomenon occurs because the structure system narrows the hydraulic cross-section of the river mouth, increasing the current speed and promoting seabed erosion. Given the short duration of the storm, bed level changes due to the storm period are not clearly visible at the end of the simulation cycle (Fig. 15(c)). However, erosion still occurs along the coast in the absence of the protection structure. When the structure is implemented, sediment deposition behind them reaches a thickness of up to 8 cm.

In coastal Segment B, accretion is predominant in all scenarios, except the central area of Segment B with the maximum erosion depth of approximately 5 cm (Figs. A.3(a), (c), and (e)). With the structures in place, deposition remains consistent along the structure line, with accretion thickness ranging from 2 to 8 cm (Figs. A.3(b), (d), and (f)). However, bottom erosion of 3 cm occurs near the T-shaped groyne at the structure system's end. For Segment C without protection system, erosion is observed along the shoreline in the NE monsoon (Fig. A.6(a)) and the Linda storm (Fig. A.6(c)), while the seabed changes show sediment deposition in the SW monsoon (Fig. A.6(e)). The presence of the structures promotes sediment accumulation behind the breakwater and causes minor erosion outside it. An average accretion thickness of 4 cm is found in the NE monsoon (Fig. A.6(b)), whereas an average sediment accumulation of around 2 cm is noted behind the breakwaters in the Linda storm case (Fig. A.6(f)).

Among the four modeled sections, Segment D experiences the most severe erosion (Fig. A.9). Severe erosion occurs along this section, with seabed erosion depths ranging from 6 to 7 cm during the NE monsoon (Fig. A.9(a)), up to 3 cm in the SW monsoon (Fig. A.9(c)) and up to 2 cm along the coast in the Linda storm scenario (Fig. A.9(e)). The presence of the protective structures generates significant localized accretion immediately behind the structures. The deposition thickness reaches up to 12 cm in the NE monsoon (Fig. A.9(b)), approximately 2.5 cm in the SW monsoon (Fig. A.9(c)) and up to 10 cm in the Linda storm (Fig. A.9(f)). However, erosion with maximum thickness of from 2 cm to 6 cm is still observed in front of the structures.

5. Conclusions

The study applied the two-dimensional MIKE 21 model to clarify the hydrodynamic characteristics and sediment transport mechanisms in the estuaries and coastal areas of Ben Tre province with the current scenario (without coastal structures) and construction scenarios (with coastal structures). The model was calibrated and validated using measured field data with quite good reliability. It effectively simulated the complex processes in this area which are governed by factors such as river flow, tides, monsoon winds and storms.

In the absence of structures, the coastal area of Thanh Phu district (Segment D) was most severely affected during both the NE and SW monsoon season. During the duration of Linda storm (1997), the coastal area of Ben Tre province was affected by storm waves with a height of less than 2.5 m. Wave heights of less than 1.0 m propagated deep into the area of river mouths. The nearshore current velocity fluctuated from 0.1 m/s to 0.8 m/s. The most severe erosion was observed in the areas of Thua Duc commune (Binh Dai district - Segment A) and Thanh Phong commune (Thanh Phu district - Segment D).

The spatial arrangement of coastal protection structures significantly affects the hydrodynamic regime and sediment transport along the coast of Ben Tre province. These structures cause wave breaking in front of them, reducing the transmitted wave heights and current speeds up to 80%. These changes lead to increase sediment deposition behind the structures along the shoreline. The sediment

accumulation is concentrated around and immediately behind the structures, with the maximum accretion thickness of 12 cm. Erosion only occur in the areas directly in front of the structures.

References

[1] Tu, L. X., Thanh, V. Q., Reyns, J., Van, S. P., Anh, D. T., Dang, T. D., Roelvink, D. (2019). Sediment transport and morphodynamical modeling on the estuaries and coastal zone of the Vietnamese Mekong Delta. *Continental Shelf Research*, 186:64–76.

[2] Tu, L. X., Duong, D. V., Tung, L. T. (2020). Assessment of coastal erosion situation, coastal protection system in the Mekong Delta and suggestion of protection solutions. *Journal of Water Resources Science and Technology*, 58:1–10.

[3] General Bathymetric Chart of the Oceans. *Gridded Bathymetry Data*. Accessed on May 10, 2023.

[4] European Centre for Medium-Range Weather Forecasts. *Browse reanalysis datasets*. Accessed on May 10, 2023.

[5] Naval Meteorology and Oceanography Command. *Western North Pacific Ocean Best Track Data*. Accessed on May 10, 2023.

[6] DHI (2014). *MIKE 21 Flow Model - Hydrodynamic Module - Scientific Documentation*.

[7] DHI (2014). *MIKE 21 Spectral Wave Module Scientific Documentation*. DHI.

[8] DHI (2014). *MIKE 21 Flow Model - Mud Transport Module - Scientific Documentation*. DHI.

[9] Moriasi, D. N., Gitau, M. W., Pai, N., Daggupati, P. (2015). Hydrologic and Water Quality Models: Performance Measures and Evaluation Criteria. *Transactions of the ASABE*, 58(6):1763–1785.

[10] Moriasi, D. N., Arnold, J. G., Van Liew, M. W., Bingner, R. L., Harmel, R. D., Veith, T. L. (2007). Model Evaluation Guidelines for Systematic Quantification of Accuracy in Watershed Simulations. *Transactions of the ASABE*, 50(3):885–900.

[11] Vu, M. T., Lacroix, Y., Nguyen, V. T. (2017). Investigating the impacts of the regression of Posidonia oceanica on hydrodynamics and sediment transport in Giens Gulf. *Ocean Engineering*, 146:70–86.

[12] Soulsby, R. (1997). *Dynamics of Marine Sands: A Manual for Practical Applications*. Report (HR Wallingford), Thomas Telford, London, UK.

[13] Nguyen, V. T. (2012). Morphological evolution and back siltation of navigation channel in Dinh An Estuary, Mekong River Delta: understanding, simulating and soluting. PhD thesis, Hohai University.

[14] Vu, M. T., Luu, C., Bui, D. Q., Vu, Q. H., Pham, M. Q. (2024). Simulation of hydrodynamic changes and salinity intrusion in the lower Vietnamese Mekong Delta under climate change-induced sea level rise and upstream river discharge. *Regional Studies in Marine Science*, 78:103749.

[15] Wölcke, J., Albers, T., Roth, M., Vorlaufer, M., Korte, A. (2016). *Integrated coastal protection and mangrove belt rehabilitation in the Mekong Delta – A pre-feasibility study for investments in coastal protection along 480 km in the Mekong Delta*. GIZ.

[16] Tran, P. C., Nguyen, V. D., Nguyen, D. C., Le, A. K., Nguyen, V. S., Mai, H. T., Duong, H. V., Lam, V. T., Tran, B. L. (2024). Research on the influence of spatial arrangement of breakwaters on the hydrodynamic regime at the coast of Ba Tri district, Ben Tre province. *Vietnam Journal of Hydro-Meteorology*, 768: 54–64.

[17] Dally, W. R., Pope, J. (1986). Detached Breakwaters for Shore Protection. Technical report, CERC-86-1, U.S. Army Engineer Waterways Experiment Station.

[18] Seiji, M., Uda, T., Tanaka, S. (1987). Statistical study on the effect and stability of detached breakwaters. *Coastal Engineering in Japan*, 30:131–141.

[19] Tanaka, N. (1976). Effects of submerged rubble-mound breakwater on wave attenuation and shoreline stabilization. In *Proceedings 23rd Japanese Coastal Engineering Conference*.

Appendix A.

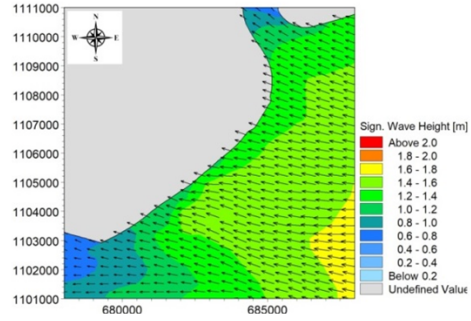

(a) NE0

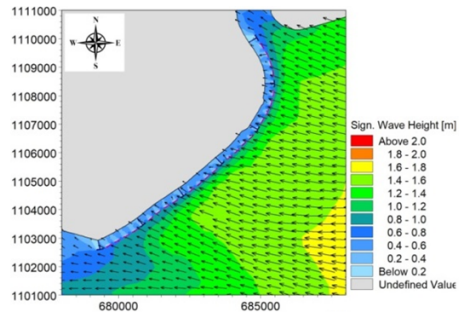

(b) NE1

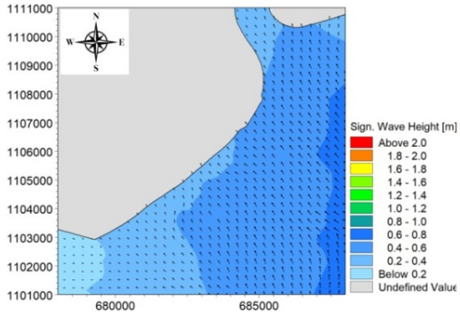

(c) SW0

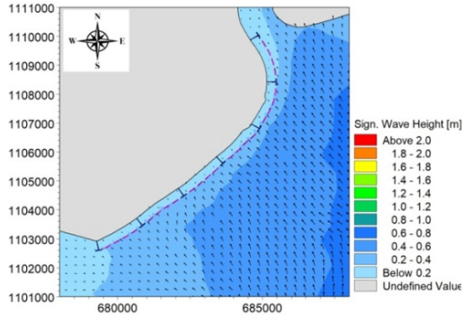

(d) SW1

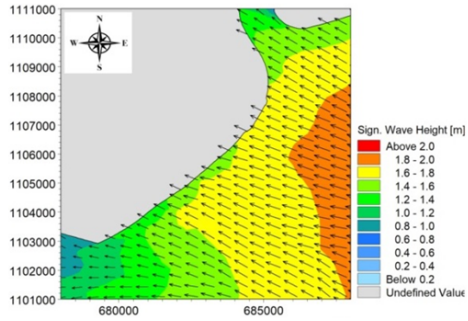

(e) Linda0

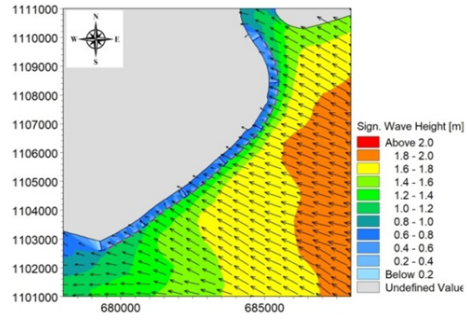

(f) Linda1

Figure A.1. Wave field in Segment B without and with protection system

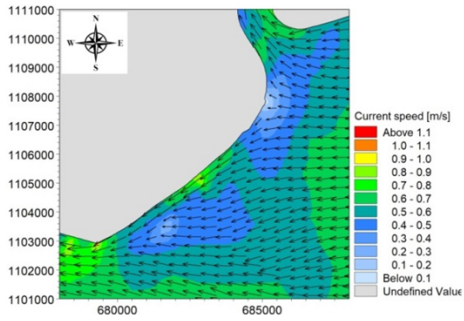

(a) NE0

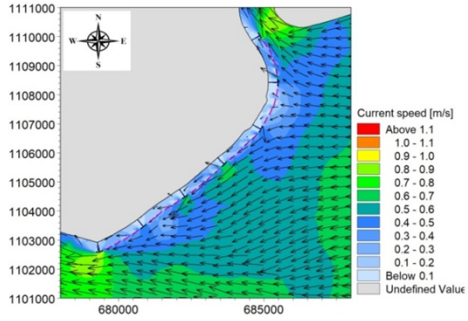

(b) NE1

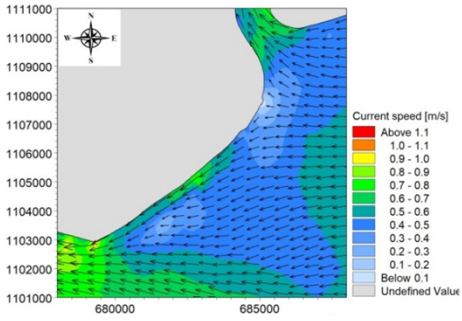

(c) SW0

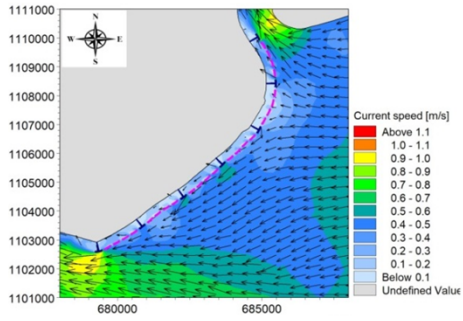

(d) SW1

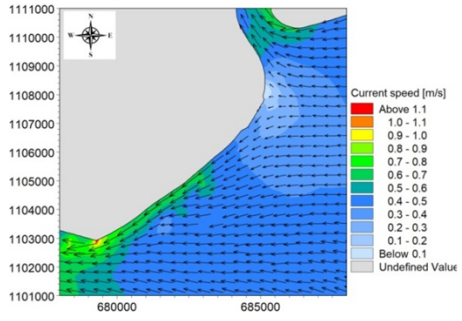

(e) Linda0

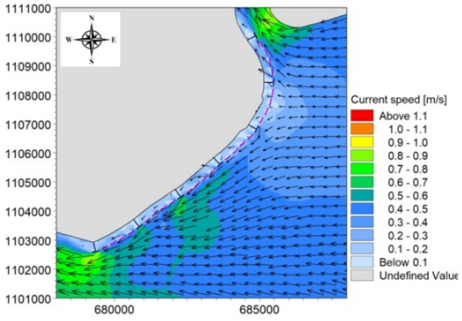

(f) Linda1

Figure A.2. Current field in Segment B during high tide without and with protection system

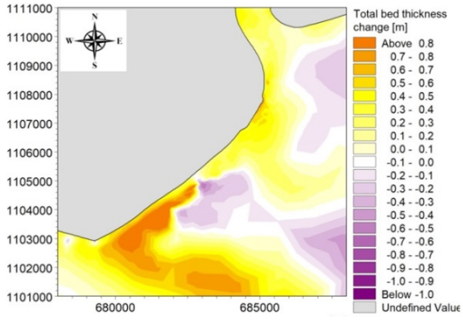

(a) NE0

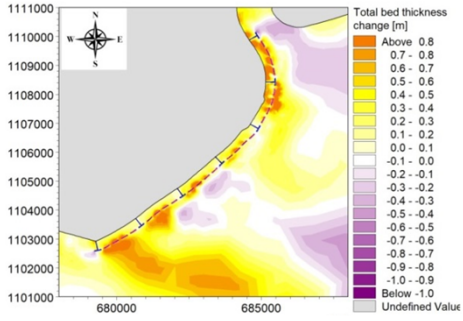

(b) NE1

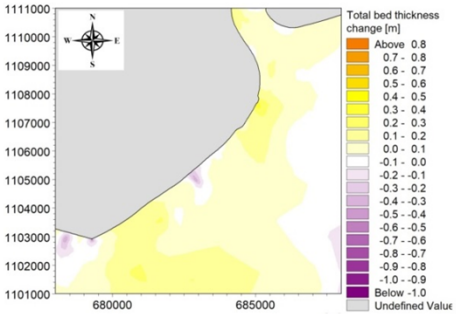

(c) SW0

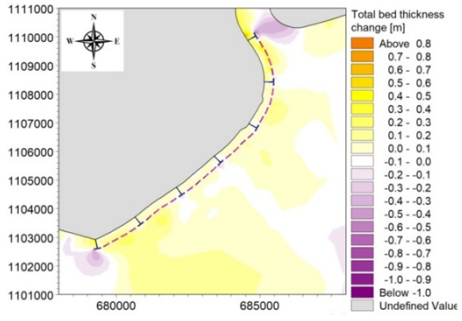

(d) SW1

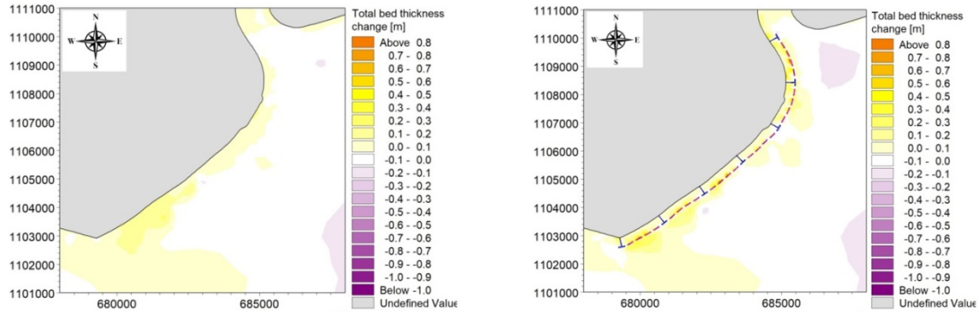

(e) Linda0 (f) Linda1

Figure A.3. Bed level changes around Segment B without and with protection system

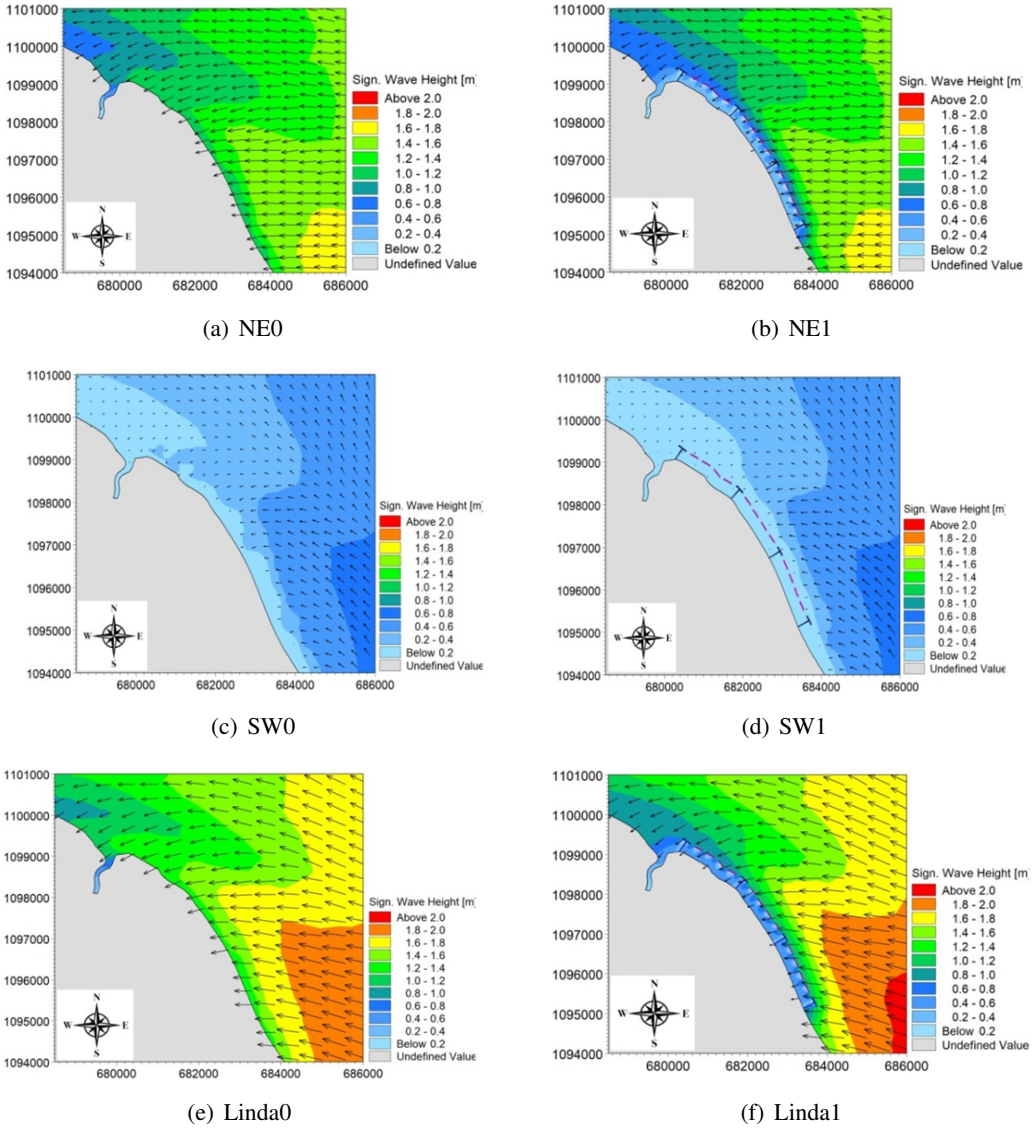

(a) NE0 (b) NE1

(c) SW0 (d) SW1

(e) Linda0 (f) Linda1

Figure A.4. Wave field in Segment C without and with protection system

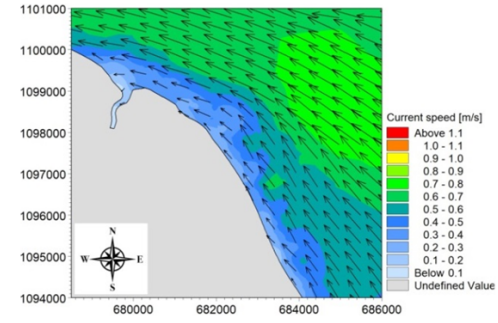

(a) NE0

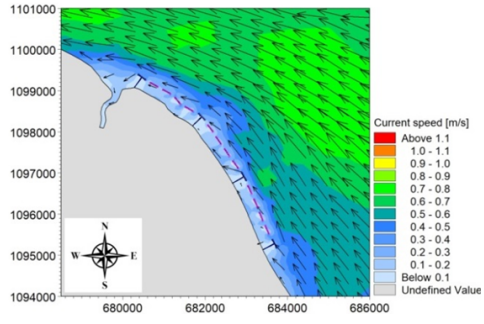

(b) NE1

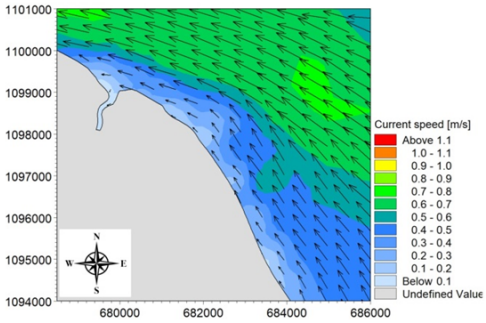

(c) SW0

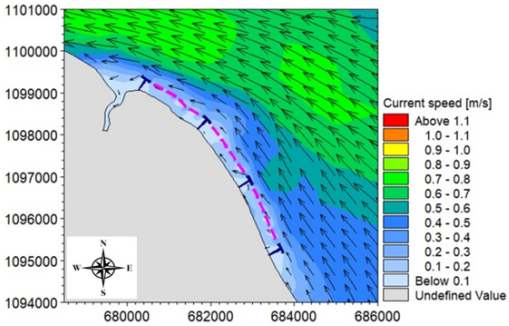

(d) SW1

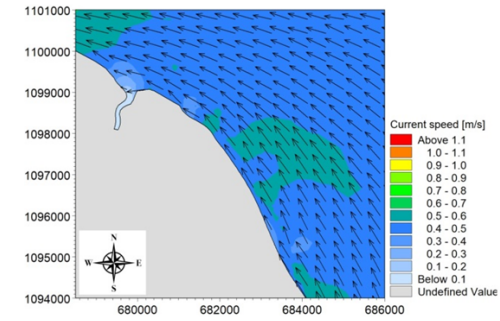

(e) Linda0

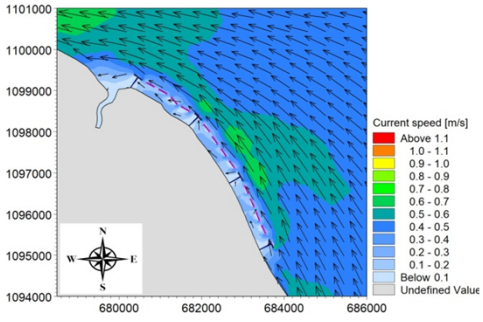

(f) Linda1

Figure A.5. Current field in Segment C during high tide without and with protection system

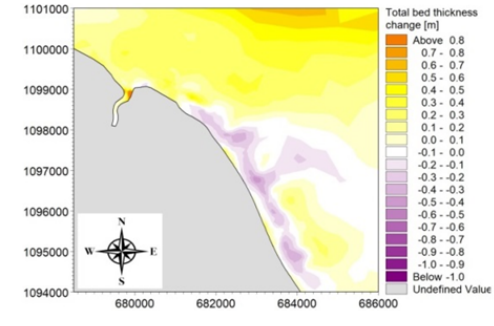

(a) NE0

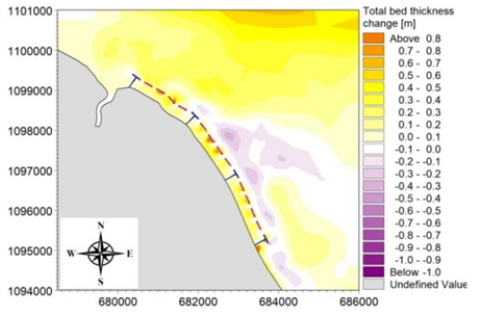

(b) NE1

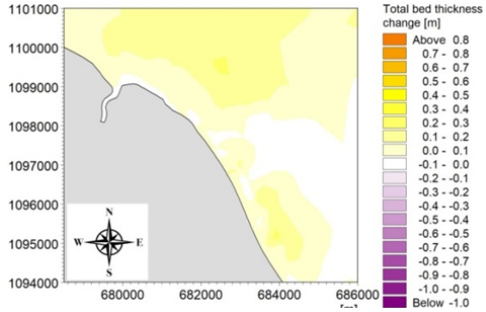

(c) SW0

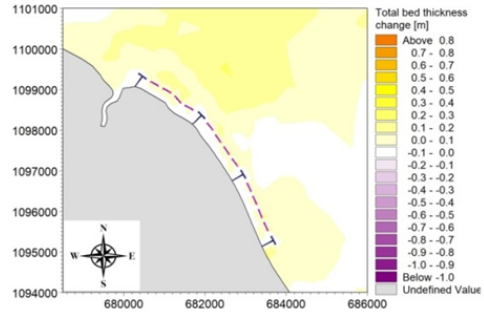

(d) SW1

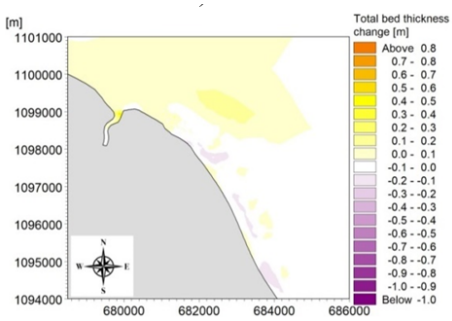

(e) Linda0

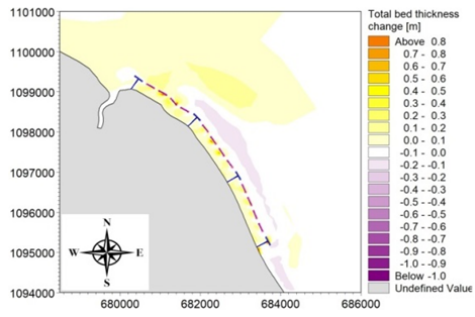

(f) Linda1

Figure A.6. Bed level changes around Segment C without and with protection system

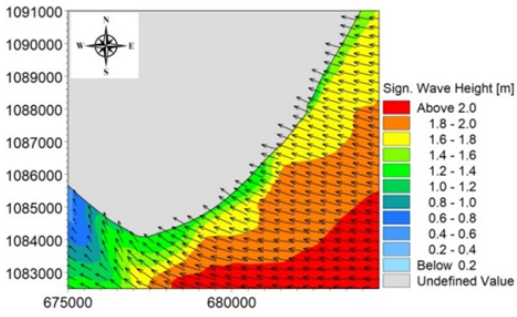

(a) NE0

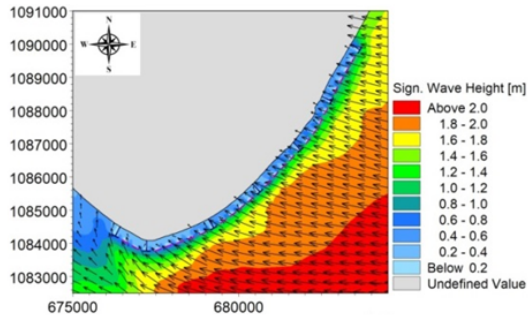

(b) NE1

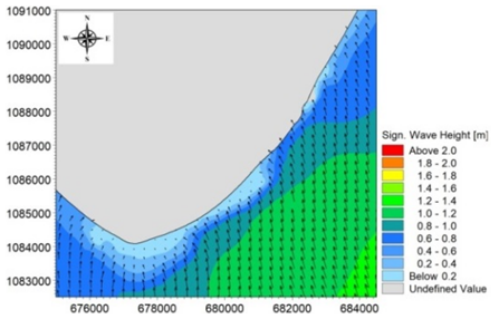

(c) SW0

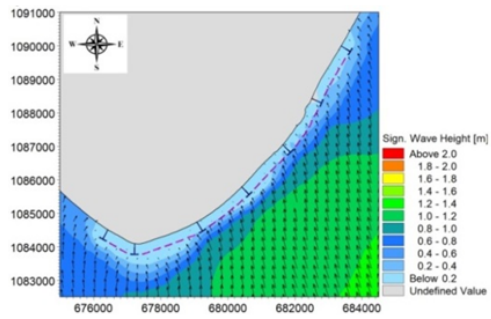

(d) SW1

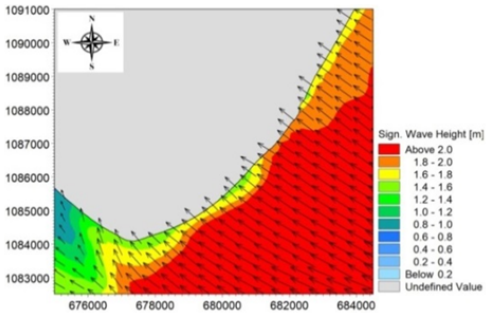

(e) Linda0

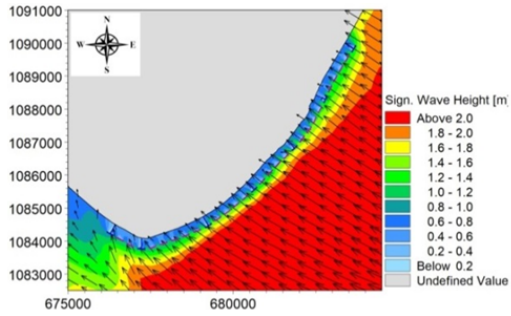

(f) Linda1

Figure A.7. Wave field in Segment D without and with protection system

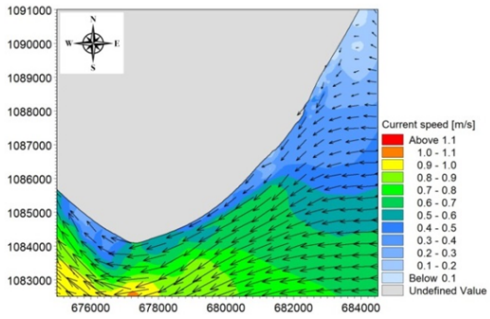

(a) NE0

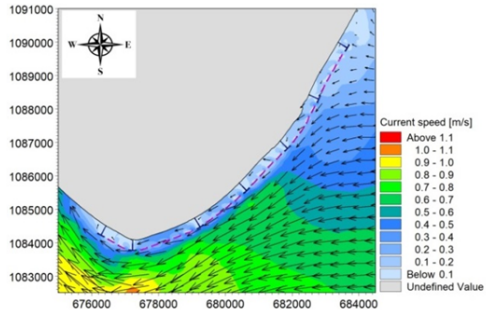

(b) NE1

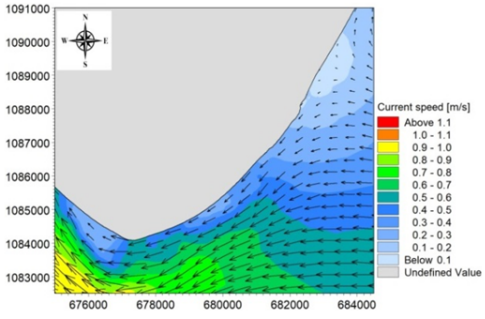

(c) SW0

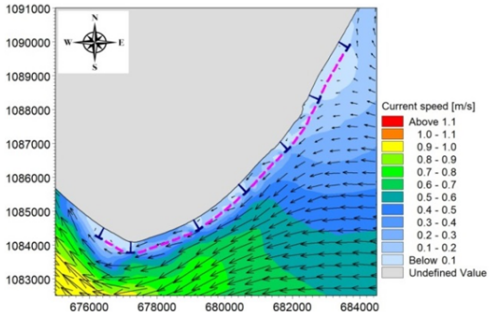

(d) SW1

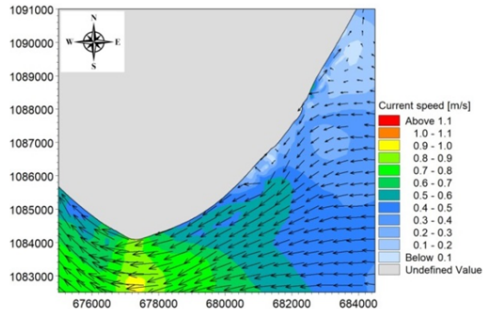

(e) Linda0

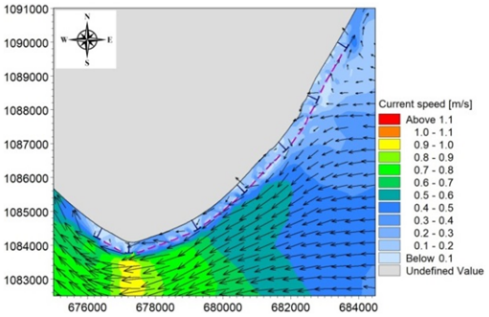

(f) Linda1

Figure A.8. Current field in Segment D during high tide without and with protection system

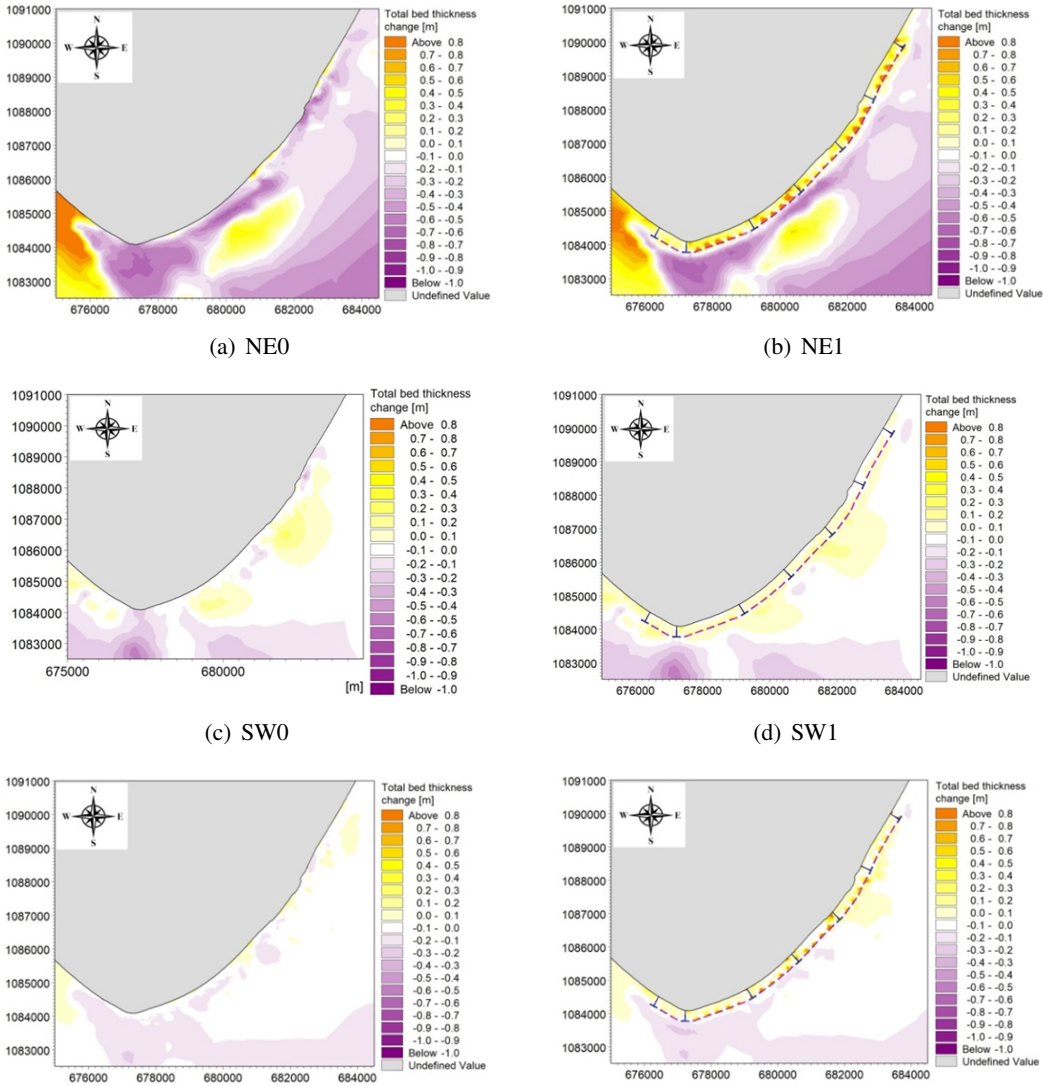

(a) NE0

(b) NE1

(c) SW0

(d) SW1

(e) Linda0

(f) Linda1

Figure A.9. Bed level changes around Segment D without and with protection system